ACS Synthetic Biology

pubs.acs.org/synthbio

Research Article

Precise Genomic Riboregulator Control of Metabolic Flux in Microbial Systems

Naresh Pandey, Steffi A. Davison, Malathy Krishnamurthy, Daniel S. Trettel, Chien-Chi Lo, Shawn Starkenburg, Katherine L. Wozniak, Theresa L. Kern, Sean D. Reardon, Clifford J. Unkefer, Scott P. Hennelly, and Taraka Dale*

Cite This: *ACS Synth. Biol.* 2022, 11, 3216–3227

Read Online

ACCESS | Metrics & More | Article Recommendations | Supporting Information

ABSTRACT: Engineered microbes can be used for producing value-added chemicals from renewable feedstocks, relieving the dependency on nonrenewable resources such as petroleum. These microbes often are composed of synthetic metabolic pathways; however, one major problem in establishing a synthetic pathway is the challenge of precisely controlling competing metabolic routes, some of which could be crucial for fitness and survival. While traditional gene deletion and/or coarse overexpression approaches do not provide precise regulation, *cis*-repressors (CRs) are RNA-based regulatory elements that can control the production levels of a particular protein in a tunable manner. Here, we describe a protocol for a generally applicable fluorescence-activated cell sorting technique used to isolate eight subpopulations of CRs from a semidegenerate library in *Escherichia coli*, followed by deep sequencing that permitted the identification of 15 individual CRs with a broad range of protein production profiles. Using these new CRs, we demonstrated a change in production levels of a fluorescent reporter by over two orders of magnitude and further showed that these CRs are easily ported from *E. coli* to *Pseudomonas putida*. We next used four CRs to tune the production of the enzyme PpsA, involved in pyruvate to phosphoenolpyruvate (PEP) conversion, to alter the pool of PEP that feeds into the shikimate pathway. In an engineered *P. putida* strain, where carbon flux in the shikimate pathway is diverted to the synthesis of the commodity chemical *cis*,*cis*-muconate, we found that tuning PpsA translation levels increased the overall titer of muconate. Therefore, CRs provide an approach to precisely tune protein levels in metabolic pathways and will be an important tool for other metabolic engineering efforts.

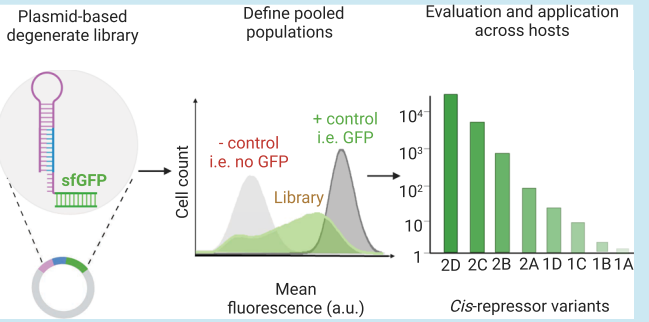

KEYWORDS: *riboregulator, RNA-based regulation, synthetic biology tools, cis-repressor, flow cytometry, metabolic engineering, cis,cis-muconate, Pseudomonas putida KT2440*

INTRODUCTION

One of the ultimate goals of synthetic biology is to re-engineer organisms to instill or reinforce desirable attributes for biotechnological applications such as the production of high-value chemicals.[1−3] For example, a great deal of effort has been performed in the field of functional metabolic engineering to enhance the production of biofuels in microbial hosts.[4−7] Balancing the energetic trade-off between microbial growth and bioproduct yield is a key challenge in the metabolic engineering field when co-opting or designing new pathways.[8−11] Although metabolic flux can be controlled through gene knockouts[12] and the coarse over- or under production of key enzymes,[13] precisely tuning protein production levels can better modulate the host's physiological needs and provide optimal parameters for bioproduction.

Various technologies have been developed as powerful tool sets for manipulating gene expression. While fine-tuning transcriptional regulators (i.e., promoters) has cemented their importance in the synthetic toolbox, other metabolic engineering tactics popular for its ability to directly tune protein synthesis levels within a pathway are ribosomal binding site (RBS) variation and RBS accessibility.[3,14−25] For example, directly tuning each enzyme in the pathway of interest by *cis*-mediated riboregulation (that act by occluding the RBS) has proven to reduce cellular burden and optimize titer, yield, and biomass in various metabolic engineering strategies (reviewed by Kent et al.[3]). In this way, a bioengineer can manipulate protein production within a metabolic engineering pathway by

Received: December 27, 2021
Published: September 21, 2022

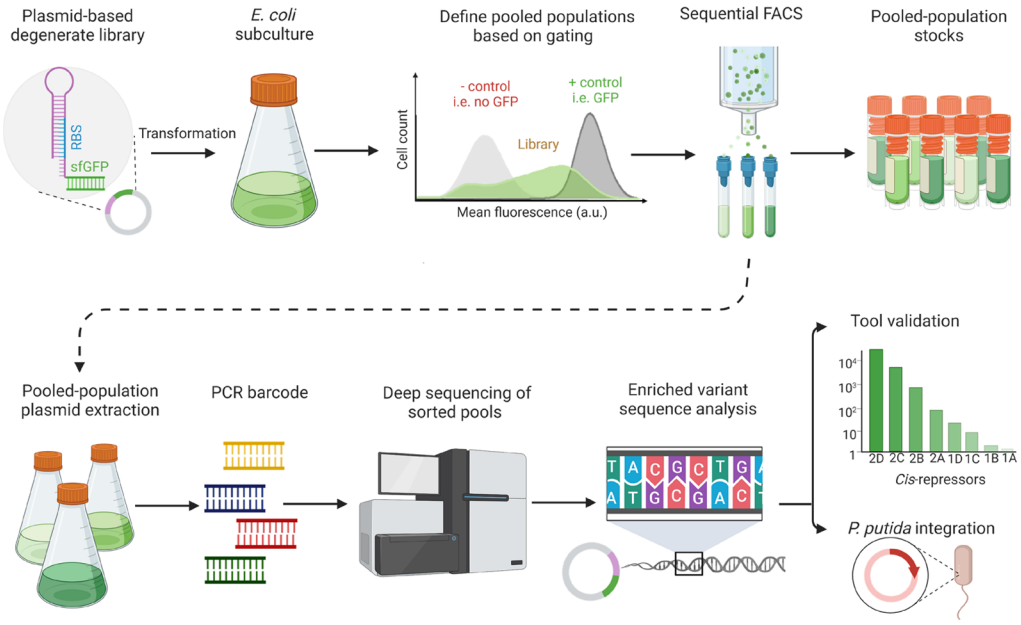

Figure 1. Workflow of CR library construction and validation. The CR design includes a *sf GFP* reporter gene downstream from a secondary structure that conceals the RBS and start codon. Using a semidegenerate library targeting the hairpin loop structure, CR variants were created, screened, and sorted by sequential FACS based on sfGFP fluorescence intensity. Plasmid DNA was extracted from eight sorted subpopulations with different fluorescence intensity levels and deep-sequenced using Miseq Illumina. Data analysis of enriched base pair positions revealed prominent CR sequences that were validated in both *E. coli* and *P. putida*. Image created with BioRender.

directly tuning down specific enzymes at the protein level, rather than at a mRNA transcript level, thus allowing for an almost digitally precise fine-tuning approach.[3,16,17,23,24,26] Additionally, because of the *cis*-acting function, there is no risk of off-target effects and no need to balance regulatory stoichiometry.

Another advantage of RNA-based technologies such as 'synthetic riboregulators,' is that they may provide a more versatile regulation to a cell compared to those that rely solely on promoter control.[17,19,22] For example, uneven translation efficiency within polycistronic transcripts have been correlated with not only proximity to the promoter[27] but also the structural accessibility of the RBS of each cistron.[28] If the RBS accessibility can be hijacked within an operon, specific targets within an operon can be more precisely tuned. However, existing RBS occlusion tools may suffer from an unpredictable dynamic range and lack of design rules for achieving optimal performance.[29] Finally, the same RBS sequence in different genetic backgrounds has been shown to lead to large differences in protein production levels.[14,30] Thus, there is a need to develop a more 'portable' design across not only genetic contexts but also coding sequence contexts. Here, we describe the development of tight protein production control that is evident in two different promoter/reporter sequence contexts, as well as different genetic backgrounds.

For this study, we utilized our previously published *cis*-repressors (CRs), which were designed to effectively block the translation of mRNA, by inhibiting the access of RBS during initiation of translation, and were further optimized to provide minimal leakage of protein production.[31] A key feature is that, unlike with previously reported riboregulators, this design achieved a large dynamic range of protein activity.[31] Moreover, we found that the regulatory loop sequence was an important design variable and fundamental to varying levels of repression.[31,32] Therefore, to further improve upon the utility of this design, we used this naturally occurring stem-loop CR sequence from our previous work[31] as the parent sequence for creating a semidegenerate library of CRs containing select, randomly mutated bases in the repressive stem-loop structure. We created 128 CR sequences with the potential to control a diverse range of protein production levels. We hypothesized that coupling this library with a highly sensitive fluorescence-activated cell sorting (FACS)-based cell isolation strategy would permit the isolation of CRs with distinct phenotypes. To this end, we developed an efficient approach to isolate these CRs, including library generation, subpopulation isolation based on a fluorescent reporter, subpopulation sequencing to identify enriched sequences, and selection of individual, new CR sequences. Then, using the new CRs at both plasmid and genomic levels, we validated CR activity by observing the control of protein production levels using superfolder green fluorescence protein (*sf GFP*)-based fluorescence[33] and chloramphenicol tolerance-based assays.

To demonstrate the potential portable nature of the selected CRs, we tested the function of the CRs across multiple contexts: plasmid-based versus genome-based, two bacterial species *Escherichia coli* and *Pseudomonas putida*), two reporter genes (*sf GFP* and chloramphenicol acetyltransferase (*CAT*)), and one native gene (*ppsA*), as well as under the control of two distinct gene expression systems (Ptac and T7A1, respectively). Finally, as a proof-of-concept application, a specific enzyme in the synthetic metabolic pathway leading to muconate production in *P. putida*[5,12] was regulated. By precisely tuning the protein production levels of the PpsA enzyme to increase PEP, a more balanced metabolic flux was achieved, resulting in increased muconate titer. Overall, our 'plug-and-play' CRs provide an easy means to precisely control protein production levels, with the advantages of tuning to extremely low levels, potentially allowing for tuning across locations within an operon and cross-context portability.

https://doi.org/10.1021/acssynbio.1c00638
ACS Synth. Biol. 2022, 11, 3216−3227

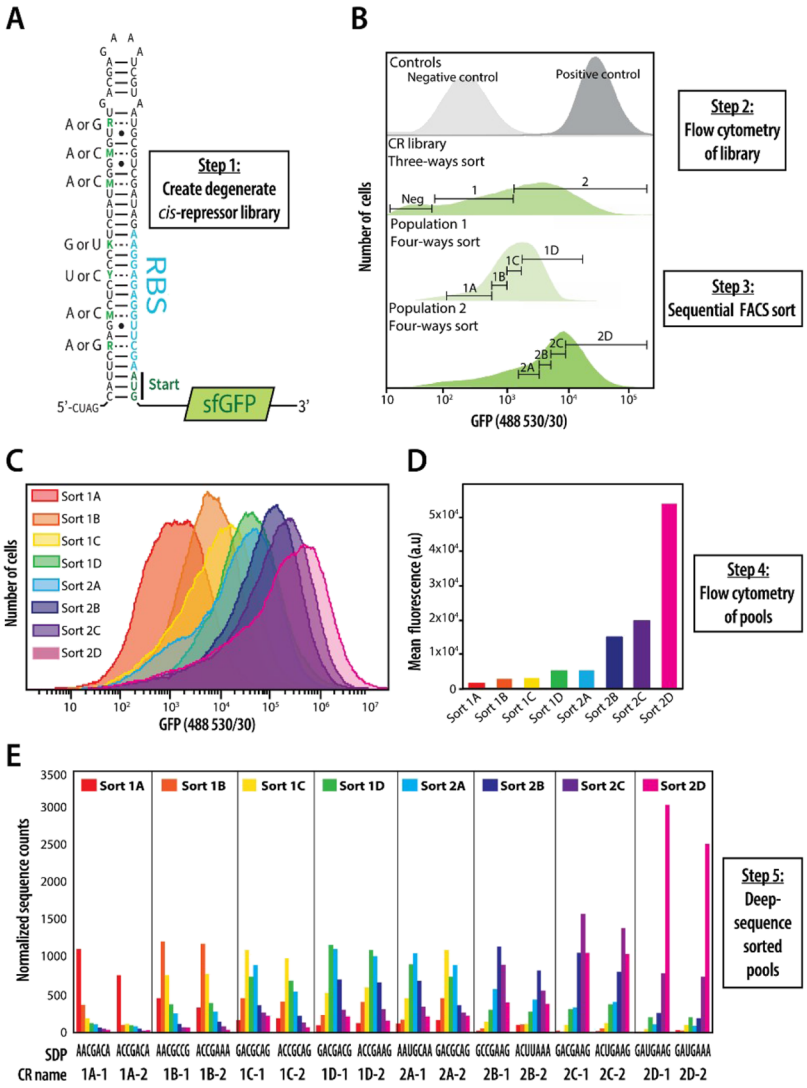

Figure 2. Cell sorting and deep-sequencing analysis of sorted pooled populations. (A) Design schematic of CR elements with variable semidegenerate positions (SDPs, green text), constrained sequences (black text), and RBS region (blue text). (B) Flow cytometry sfGFP fluorescence histograms for the CR library compared to positive (dark gray, sfGFP vector with no CR sequence) and negative (light gray, DH5α cells without vector) controls. (C) Analytical flow cytometric measurements for each sorted population after a 16 h incubation from an inoculation at OD_{600} 0.05. (D) Analytic flow cytometric measurements for each sorted population after a 24 h cultivation directly inoculated from a glycerol stock. (E) Sequence enrichment analysis of each sorted pool after deep sequencing.

RESULTS AND DISCUSSION

Overview of CR Library Construction and Validation.

The field of synthetic biology is lacking universal genetic tools that can precisely regulate protein production levels to manipulate flux through biosynthetic pathways. Thus, our goal was to create an RNA-based design to control cellular networks that are mostly dominated by protein-based components. To accomplish this, we first established a CR DNA library. Second, we used FACS to isolate subpopulations of varied phenotypes, based on the fluorescence of sfGFP. Third, we analyzed the CR sequences of the subpopulations and finally, we selected and characterized a subset of individual CR sequences. An overview of the workflow is presented in Figure 1.

Our previously described CR design, CR-4, was used as a starting hairpin structure.[31] CR-4 contains a 34 bp stem loop that effectively occludes the RBS, thus preventing translation of downstream genes. To create a diversity of protein production profiles based on CR-4, a library of CR sequences with the potential for mismatched base-pairs in the stem loop at seven specific positions were chosen based on Krishnamurthy et al.[31] Thus, 128 permutations were designed and inserted into the pCK vector[34] to control the translation level of the reporter *sfGFP* gene (Figure 2A). These newly constructed pCKCRlib (pCK CR library) vectors were transformed into *E. coli* for further testing as a single, bulk population. The population of CR variants was observed to have a broad range of sfGFP fluorescence intensities, demonstrating that the library design successfully created a range of CR knockdown activities, from full repression to unrepressed, when compared to the negative and positive controls (Figure 2B).

After overnight cultivation, eight distinct fluorescent phenotypes from the library of CR variants were isolated by FACS using two sequential sorting steps. First, the library population was sorted 'three-ways', resulting in Populations NEG, 1, and 2 (Figure 2B and Supplementary Figure S1, Table S1). The NEG population represented 'negative' (dark) cells in

https://doi.org/10.1021/acssynbio.1c00638
ACS Synth. Biol. 2022, 11, 3216−3227

the CR population, showing fluorescence intensity levels even lower than the negative control (Figure 2B). Potential reasons for this phenotype include: the cells (1) contain a CR variant(s) responsible for complete protein production inhibition, (2) did not grow well, or (3) have no plasmid content thus providing no genotypic data. Because we could not unravel these possibilities, we discarded the NEG population (~10% of the population) and moved forward only with Populations 1 and 2 (Figure 2B). Then, Population 1 and Population 2 were each sorted 'four-ways' and labeled A through D, thereby creating eight isolated subpopulations of CR variants: 1A, 1B, 1C, 1D, 2A, 2B, 2C, and 2D (Figure 2B, Supplementary Figure S1). More detailed flow cytometry graphs and statistics tables can be viewed in the Supplementary File.

The successful isolation of distinct CRs within a defined subpopulation of cells by in vitro fluorescence analysis of the combinatorial library (i.e., 128 permutations in this study) depends on the stability of the subpopulation phenotypes. To test the stability of our eight subpopulations, 1A−1D and 2A−2D, each subpopulation was cultured overnight directly after FACS. Then, the next day, the cultures were analyzed by flow cytometry (Figure 2C, Table S2), and glycerol stocks were created from these populations. The flow cytometry results showed increasing fluorescence intensity of the eight subpopulations across nearly three logs, with 1A being the most repressive and 2D being the least repressive (Figure 2C), consistent with the expected fluorescence intensity values based on the gates used for sorting. Furthermore, the populations continued to demonstrate a >100-fold range of fluorescence profiles after a 24 h cultivation from a glycerol stock inoculum (Figure 2D, Supplementary Figure S4, Table S2), indicating that the CR variants in each subpopulation consistently regulated sfGFP production to varying levels.

To identify the CR variant sequences responsible for each subpopulation phenotype, the plasmid vectors were purified from each defined pool and were PCR-barcoded (Supplementary Table S3) for deep sequencing by Illumina MiSeq. Data analyses were performed to identify the enriched variant sequence regions (Figure 2E). Reads for each pool (~38,000/pool) were analyzed for sequences whose population was enriched within each pool. Two distinct CR sequence examples, those showing enrichment in a given subpopulation but were represented to a lesser or no degree in the other subpopulations, were selected from each subpopulation based on these analyses (totaling 16 sequences). Notably, the sequences for 1C1 and 2A2 were identical; thus, only 1C1 was used in subsequent experiments.

Validation of CRs with Discrete Phenotypic Profiles in *E. coli*. Utilizing the 15 selected CR elements, plasmid-based constructs of the individual CRs directly upstream of *sf GFP* and *CAT* genes were tested in *E. coli*. Analytical flow cytometry measurements quantified the level of CR-sfGFP production (Figure 3A). The fluorescence intensity of the defined CR sequences based on the deep-sequencing analysis (Figure 3A) corresponded to the fluorescence intensity results obtained from the eight sorted subpopulations shown in Figure 3A, demonstrating that the ranking order of protein production levels from the individual CR sequences is similar to the order of sfGFP activity levels in the subpopulations.

To further confirm that the selected CR sequences result in a spectrum of protein production levels, a *CAT* assay in *E. coli* was performed. The expectation was that the repression activity of the different CRs would differentially confer susceptibility of the cells to chloramphenicol (Cm). Ten CRs were analyzed in the *CAT*/Cm tolerance assay. As expected, the ranking of chloramphenicol resistance by CR was similar to the sfGFP Fl results (Figure 3A, Supplementary Figure S5). For example, the CRs with higher repression activity, 1A1 and 1B1, demonstrated no growth at 30 μg/mL

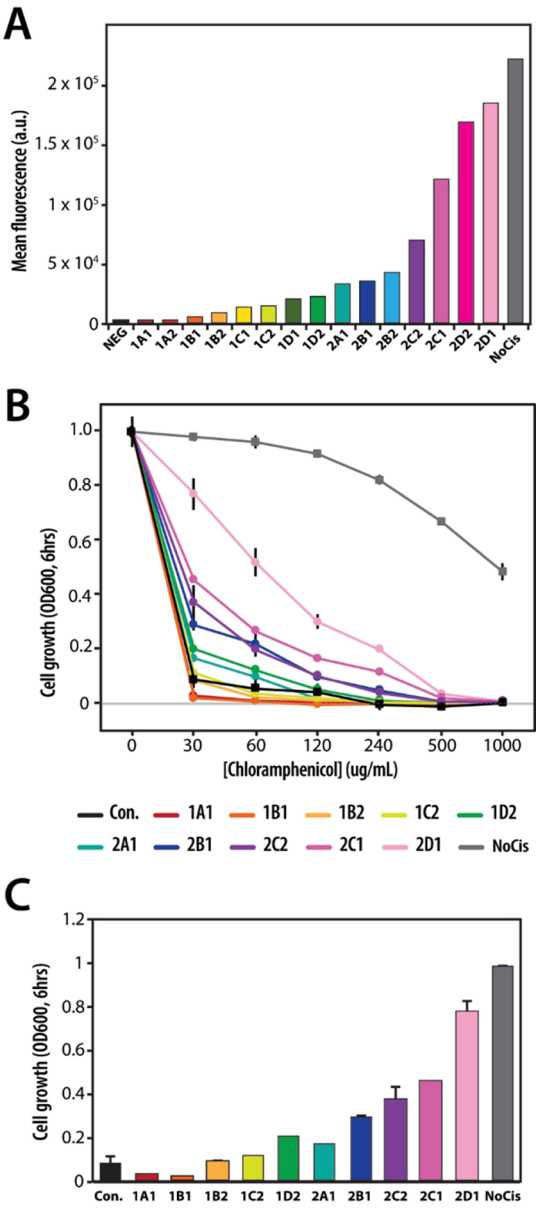

Figure 3. Fluorescence intensity and growth profiles of *cis*-repressed *E. coli* transformants. (A) Analytical flow cytometry results for the 15 unique CR sequences in *E. coli* transformants, each containing a different *cis*-repressed sfGFP vector under Ptac promoter control. Control strains were *E. coli* cells lacking transformed CR plasmid (NEG) or those transformed with a vector containing the *sf GFP* gene with no CR regulation (NoCis). (B) Normalized cell growth of *E. coli* transformants containing 10 different CRs in front of the *CAT* gene under T7A1 promoter control, cultivated in different concentrations of chloramphenicol (Cm). Control strains were*E. coli* cells lacking transformed CR plasmid. (C) *E. coli* transformants containing *cis*-repressed CAT after 6 h cultivation in Lysogeny Broth (LB) media supplemented with 30 μg/mL Cm. The error bars represent standard deviations from the mean of biological triplicates.

https://doi.org/10.1021/acssynbio.1c00638
ACS Synth. Biol. 2022, 11, 3216−3227

Cm after 6 h cultivation, suggesting the weakest protein production levels of *CAT* compared to the other transformants (Figure 3C). By contrast, a high Cm tolerance was demonstrated by the construct 2D1, with normalized cell growth up to 0.7 OD_{600} after 6 h cultivation. Based on the cell growth profile, the 2D1 construct demonstrated a 20% decrease in cell growth (OD_{600}) compared to the control strain that has no CR (NoCis) driving *CAT* protein production levels (Figure 3B). Together, these results demonstrate a large dynamic range of protein production regulation for two distinctly different reporter genes (*sfGFP* and *CAT*) and promoter systems (Ptac and T7A1, respectively), with clear reproducibility and near digital control of protein production from a very low level to an "all-on" high level.

Establishing CRs in *P. putida*. To test the cross-strain portability of the new CRs, a subset of five CRs, 1A1, 1C2, 2B1, 2C1, and 2D1 were tested in *P. putida*. The CR-*sfGFP* expression constructs were cloned into the pBTL-2 vector with the constitutive Ptac promoter driving transcription. Plasmids were transformed into *P. putida* KT2440 resulting in strains NP230, NP231, NP232, NP233, NP234, and NP235 for CRs 1A1, 1C2, 2B1, 2C1, 2D1, and NoCis, respectively. Fluorescence from each strain was compared to the positive and negative controls, "NoCis" construct without CR regulation (NP235) and an empty vector construct without the *sfGFP* gene (NP240), respectively. As expected, the unrepressed sfGFP construct (NoCis) demonstrated the highest fluorescence intensity among all strains tested, and the fluorescence intensity decreased with increasing strength of the CRs, as expected (Figure 4A). By contrast, the fluorescence intensity of the strongest CR-1A1 showed no difference to the negative control (pBLT-2) which lacked *sfGFP* gene (Figure 4A). Notably, the ranking of the fluorescence intensity of CRs was similar in *P. putida* (Figure 4A) and *E. coli* (Figure 3A), demonstrating consistent performance across both bacterial species and highlighting a future potential use of CRs as an agnostic bacterial tool. Further applications of CRs in diverse hosts will be needed to test the extent of how broadly agnostic CRs are with respect to host background, genome position, upstream promoter, and effected gene, especially within a native operon context.

The CR-*sfGFP* constructs were next evaluated within the *P. putida* genome to confirm that their performance is consistent when integrated in the genome versus plasmid-based. The same subset of CR-sfGFP constructs (1A1, 1C2, 2B1, 2C1, 2D1, and NoCis) driven by the Ptac promoter were integrated at the PP_2684-PP_2685 locus of KT2440, resulting in strains NP241, NP242, NP243, NP244, NP245, and NP246, respectively. The level of fluorescence intensity observed in the genomic-expressed constructs (Figure 4B) was markedly lower compared to the plasmid-based expression (Figure 4A), most likely because of the decreased copy number.[37] However, the fluorescence intensity ranking between the constructs for the genomic-expressed CR-*sfGFP* was similar to the plasmid-based system (Figure 4). For example, the highest fluorescence intensity was observed in the strain without any CR present (NoCis), with fluorescence intensity decreasing with increasing strength of the CRs (Figure 4). Again, the strain with the strongest CR element, NP241 (CR-1A1), had no significant difference in fluorescence intensity compared to the wildtype KT2440 (Figure 4). Thus, consistent performance from both plasmid and integrated CR elements was observed.

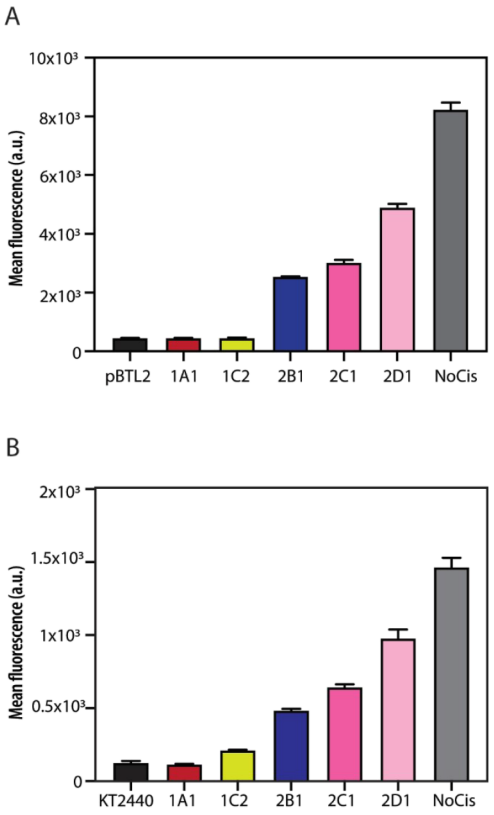

Figure 4. Profiles of repression were consistent between plasmid-based and genomic reporters in *P. putida* KT2440. (A) Fluorescence intensity profiles of transformants with pBTL-2-based plasmids with various CRs controlling the protein synthesis levels of sfGFP. (B) Fluorescence intensity profiles of the transformants with integrated CRs controlling the protein synthesis levels of sfGFP at the PP_2684-85 locus. The error bars represent standard deviations from the mean of biological triplicates.

Using CRs to Tune a Metabolic Pathway in the Muconate-Producing *P. putida* CJ442. The CRs were then applied to the muconate production pathway, to determine if they can affect the production of a commodity chemical, muconic acid (MA or muconate). We chose *Pseudomonas putida* strain CJ442 as a parent strain because of its successful muconate production[12,35] and our previous experience with this system.[36−38] *P. putida* has been identified as a good host for the metabolic conversion of glucose and lignocellulosic biomass (e.g., agricultural byproducts) into the commodity chemical muconate, via the introduction of new and co-opted metabolic pathways[5,6,12,35,39] (Figure 5). Johnson et al.[12] demonstrated that the deletion of the *P. putida* genes *pgi-1/2*, *pykA/pykF*, and *ppc* in the strain CJ442 diverted carbon flux toward the shikimate pathway; carbon is then shunted toward protochatechuate using heterologous enzymes AsbF (a 3-DHS dehydratase) and AroY/EcdB (a protocatechuate decarboxylase), which produces catechol and subsequently muconate by the *catA* gene. At the expense of cell growth, pyruvate and adenosine triphosphate (ATP) are utilized by the phosphoenolpyruvate synthase enzyme (PpsA) to synthesize phosphoenolpyruvate (PEP), an important precursor in muconate biosynthesis. Therefore, this reaction is an important metabolic link between the tricarboxylic acid (TCA) cycle and muconate production in *P. putida*.[40] Ultimately, the phosphoenolpyruvate synthase (*ppsA*) gene was targeted for *cis*-repression, in order

https://doi.org/10.1021/acssynbio.1c00638
ACS Synth. Biol. 2022, 11, 3216−3227

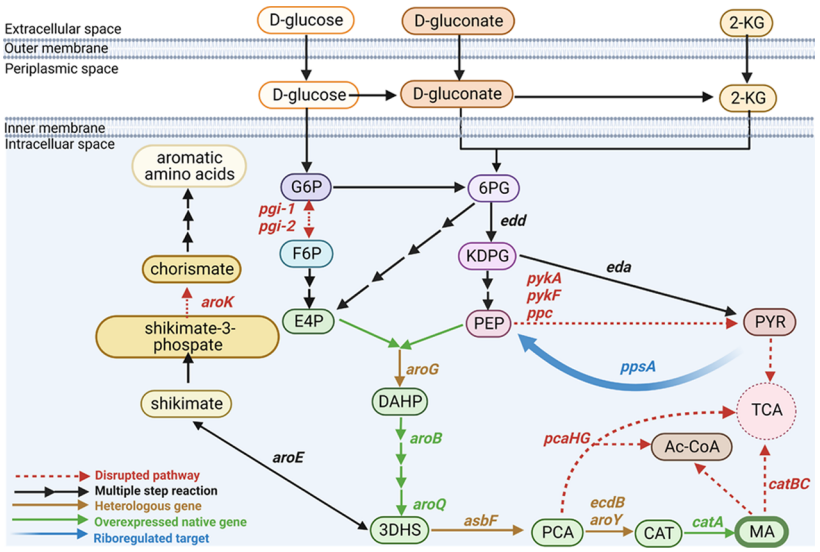

Figure 5. Metabolic pathway for muconate production in engineered *P. putida* CJ442. Abridged metabolic pathway adapted from the comprehensive metabolic map in Bentley et al.[35] Deleted genes are shown in red; heterologous genes are shown in brown; native genes that are overexpressed are shown in green. The riboregulated protein phosphoenolpyruvate synthase enzyme (PpsA), which converts PYR into PEP, is shown in blue, and its flux is demonstrated with a blue arrow (gradient represents tuning of overexpression using CRs in this study). Multiple-step reactions are indicated by multiple arrows. See more details in the Materials and Methods section. Image created with BioRender.com.

to modulate its protein expression levels, because the PYR + ATP → PEP reaction is an important metabolic link between the TCA cycle and muconate production in *P. putida*[40] (Figure 5). However, initial attempts to 'tune' the expression of the gene *ppsA* to balance growth and muconate production failed, due to the transcriptional regulation of a PEP synthase regulatory protein gene (PP_2081) that is located upstream of *ppsA*.[40,41] Thus, PpsA could theoretically benefit from being precisely controlled to retain sufficient pyruvate levels for growth while still shunting carbon toward PEP, analogous to a similar effort in the *E. coli* shikimate production pathway.[42]

To generate *P. putida* strains with CR-regulated PpsA, an integration strategy was adopted which simultaneously deleted the promoter region of, and integrated individual CRs in front of, the *psrp* gene. Our original intent was to use the same CRs that were tested in Figure 4. However, attempts at integrating the less-repressive CR-2C2 and CR-2D1 elements in front of the PSRP gene were unsuccessful. This result is potentially because our genomic CR system is driven by the highly expressing Ptac promoter, rather than *psrp*'s native promoter, leading to overexpression of the gene. Overexpression of PpsA can cause PEP accumulation and depletion of the pyruvate pool, which has been suggested to lead to poor growth.[43−46] Therefore, we chose four CRs with higher repression activity, 1A1, 1C1, 1D1, and 2B2, still with the goal of testing whether tuning PpsA production levels can alter growth and muconate production in *P. putida*.

After evaluating the growth, muconate titers, glucose consumption, and 2-ketogluconate (2-KG) accumulation of the *cis*-repressed PpsA strains NP185, NP186, NP187, and NP188 (Figure 6), it was evident that tuning phosphoenolpyruvate synthase production level does affect both growth and muconate production (Figure 6). NP185 (CR-1A1, most repressive) has a phenotype similar to the non-CR-regulated strain CJ442, indicating that the remaining, less-repressive CR-regulated strains overexpressed PpsA relative to the native system in CJ442. Consistent with this, NP186 and NP187, with the 1A1 and 1C1 CRs respectively, demonstrate phenotypes similar to each other but different from CJ442. In both cases, the cultures grew more slowly, showed slower glucose uptake rates, and showed a delayed 2-KG accumulation profile. Muconate accumulation rates were also slower; however, the final muconate titers were improved for both of these CR-regulated strains. NP188 (CR-2B2) showed significantly delayed growth, as well as a markedly slower muconate accumulation rate relative to the other strains, again possibly because of the accumulation of PEP at the expense of pyruvate. Taken together, these results indicate that increasing PEP formation at the expense of growth has the potential to increase final muconate titers. However, a threshold potentially exists, whereby significant overexpression of the *ppsA* gene may prove to critically deplete the pyruvate pool,[45,47,48] as we observed with NP188 (Figure 6). Importantly, the ability of CRs to fine-tune the protein synthesis levels of sensitive enzymes is indicative of its advantage over the traditional overexpression method, which may be deleterious toward the product yield and the cell's viability. This novel titration-based method demonstrates the utility of CRs in balancing the metabolic flux without creating a harmful burden on the cells.

In the muconate production pathway in *P. putida*, not all of the 'ON' target pathway enzymes need to be expressed at a maximum level and, more often than not, these high-level expressions can cause unnecessary burdens for the host metabolism, such as an accumulation in intermediates such as 2-KG.[35] In general, when exogenous genes are introduced into cellular pathways/network, a 'trade-off' in metabolic burden for the cells is observed, that is, limited growth and overall productivity.[12,35] Likewise, 'OFF' target pathway genes cannot be repressed at too low of levels without detrimental consequences.[12] Furthermore, in a balanced cellular network, each enzyme production level is dictated by its stability, activity, maturity, and turnover for performing its function.[49] Therefore, tuning protein synthesis levels to achieve optimum enzyme levels may be beneficial for cellular metabolism where resources can be redirected for optimal productivity and healthy cellular growth.[19] However, a challenge of fine-tuning

https://doi.org/10.1021/acssynbio.1c00638
ACS Synth. Biol. 2022, 11, 3216−3227

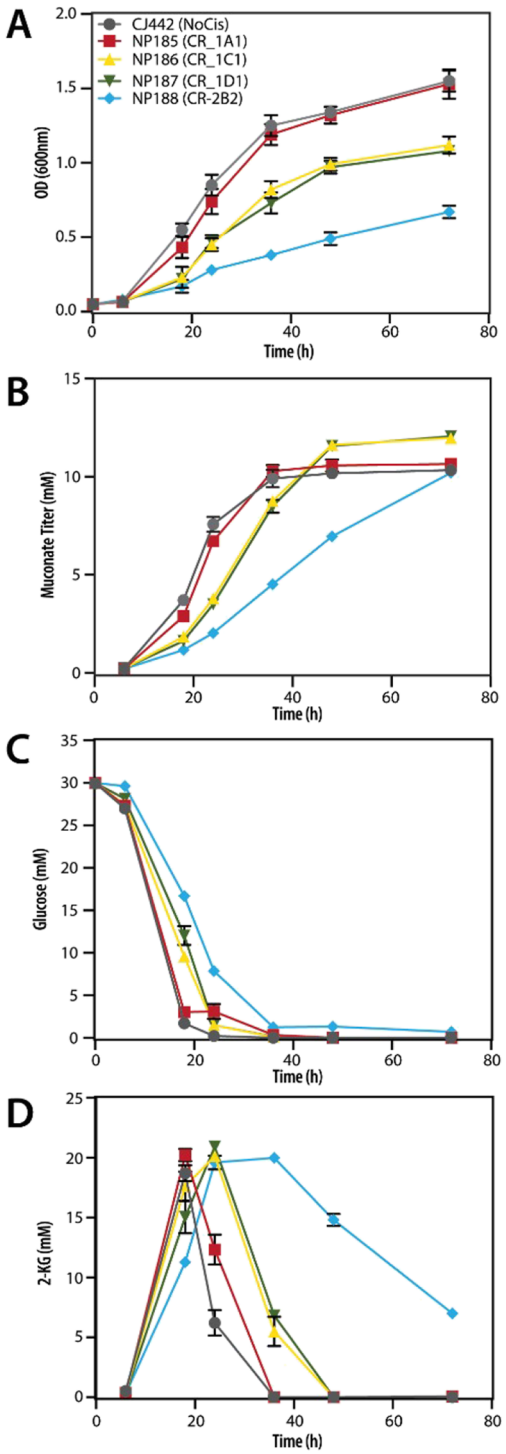

Figure 6. Effect of tuning *PpsA* overexpression in *P. putida* CJ442 using CRs. (A) Growth curves, (B) muconate titers, (C) glucose consumption rates, and (D) build-up of the intermediate 2-ketogluconate (2-KG) of *P. putida* transformants, namely, CJ442 (black circles, NoCis), NP185 (red squares, CR-1A1), NP186 (yellow triangles, CR-1C1), NP187 (green reverse triangle, CR-1D1), and NP188 (blue diamonds, CR-2B2) measured by a shake flask experiment. The error bars represent standard deviations from the mean of biological triplicates.

the protein production levels includes the potential for extensive testing of protein production levels for each enzyme in the pathway. In addition, initial checks are generally not performed to determine if overexpression constructs are causing a metabolic burden for cells once the goal of product formation is achieved.

Importantly, the CR elements described here are agnostic to the gene being controlled, only requiring the ATG start codon from the coding sequence to function properly. In contrast to traditional riboregulators that required an additional activation step,[7,12,35−37] the CRs created in this study do not require activation. The CR activity also does not seem to depend upon the upstream or downstream sequence (i.e., from promoter to gene), allowing for a seamless incorporation into any design without need for further analysis to ensure proper expression.[30] Other advantages to this design include the potential portability feature and reduced labor-intensive screening time usually required for inducers and/or external stimuli.[40] Therefore, this 'plug-and-play' system can be incorporated into the design of the CRs whereby multiple CRs can be tested to achieve the best protein production level profile.

In summary, the riboregulators described here have been applied to synthetic biology and metabolic engineering. Additionally, the utility of CRs can be expanded beyond a stand-alone expression system, without any need for an inducer due to the built-in set threshold for protein synthesis allowing for ease of portability. Furthermore, these RNA-based engineering efforts were successfully applied for a biotechnological application in altering metabolic flux toward the production of a value-added chemical, *cis*,*cis*-muconate, by dialing in the protein levels of PpsA. Taken together, this work provides a toolbox of components and validated workflows for implementing CRs where precise expression of specific enzymes is required in *P. putida*. Although a small library of 128 variants was used in this study, the use of FACS for cell sorting opens the possibility of screening much larger (10^4−10^6) libraries in future work. More broadly, these efforts establish a framework for further development of regulatory tools for tuning translation levels to very low levels in industrially promising bacteria.

MATERIALS AND METHODS

Growth Conditions and Strains. *E. coli* and *P. putida* cultures were grown in LB medium (Merck) or 1× M9 medium[35] (without trace elements), supplemented with 50 μg/mL kanamycin (Kan50) (Merck) when necessary to maintain plasmids. Transformants were selected on LB agar plates containing 10 g/L tryptone (Fischer), 5 g/L yeast extract (Biochemika), 5 g/L NaCl (Sigma), and 15 g/L agar (Sigma), supplemented with Kan50 and grown overnight at 37 or 30 °C for *E. coli* or *P. putida*, respectively. The cultures were cultivated in 15 mL round-bottom culture tubes (BD falcon) in a volume of 3−5 mL at 30 °C (*P. putida*) or 37 °C (*E. coli*) with shaking at 225 rpm. For analysis of muconate production, transformants were cultivated in 1× M9 medium, which consists of 6.78 g/L Na_2HPO_4 (Fischer), 3 g/L KH_2PO_4 (Sigma), 0.5 g/L NaCl (Sigma), 1 g/L NH_4Cl (Sigma), 2 mM $MgSO_4$ (Acros), 100 μM $CaCl_2$ (Fischer), 18 μM $FeSO_4$ (Sigma), and 30 mM glucose (Sigma).

The NEB5α competent *E. coli* (New England Biolabs) was used for cloning of the plasmids. The replicative vector pBTL-2 vector backbone was used for *P. putida* replicative vector construction (Supplementary Table S4). *P. putida* KT2440 (ATCC #47054) derivatives were used for plasmid transformations and genomic integration of *cis*-repressed *sfGFP*, whereas the *P. putida* strain CJ442[12] was used for genomic

https://doi.org/10.1021/acssynbio.1c00638
ACS Synth. Biol. 2022, 11, 3216−3227

integration of *cis*-repressed *ppsA* (listed in Supplementary Table S4). As shown in the metabolic pathway map for CJ442 (Figure 5), the deletion of glucose-6-isomerase (encoded by *pgi-1* and *pgi-2*) interrupted the EDEMP cycle (i.e., recruiting activities from the ED, EMP, and PP pathways) and directed carbon flux toward erythrose-4-phospate (E4P).[12] The 6-phosphogluconate (6PG) is dehydrated to 2-keto-3-deoxy-6PG (KDPG), which is cleaved by 2-keto-3-deoxy-6-phosphogluconate aldolase to gyceraldehyde-3-phosphate and pyruvate (PYR) (the first two steps of the Entner−Doudoroff pathway) (not pictured). Erythrose-4-P (E4P) along with a 5-carbon sugar phosphate is produced from the recombination of gyceraldehyde-3-phosphate and fructose-6-phosphate (F6P) via a transaldolase/transketolase (not pictured). Phosphoenolpyruvate (PEP) is made from the pyruvate (PYR). PEP competition is reduced by deleting pyruvate kinase (encoded by *pykA* and *pykF*) and pyruvate carboxylase (encoded by *ppc*) inhibiting the carbon flow to acetyl-CoA and the TCA cycle. Furthermore, the catabolic genes downstream of MA, *catBC*, and the regulator *catR* are deleted. PEP is directed to MA via expression of a feedback resistant 3-deoxy-D-arabinoheptulosonate (DAHP) synthase (encoded by *aroG* derived from *E. coli*) followed by overexpression of a 3-dehydroshikimate (3DHS) dehydratase (encoded by *asbF* derived from *Bacillus cereus* ATCC 14579), which generates protocatechuate (PCA) from 3-deoxy-D-arabinoheptulosonate 7-phosphate (3DHS). To convert PCA to catechol (CAT), a PCA decarboxylase (encoded by *aroY* derived from *Enterobacter cloacae* ATCC 13047) and the corresponding accessory protein that generates the prenylated flavin cofactor (encoded by *ecdB* derived from *Enterobacter cloacae* ATCC13047) are overexpressed. The native *catA* is overexpressed to CAT to MA. Deletion of *aroK* terminates the shikimate pathway.

Semidegenerate Library Construction and FACS of CR Elements. A library of CR elements was inserted in front of the *sfGFP* gene for selection. The library was derived from the CR-4 *cis*-repressor element previously reported.[31] A DNA ultramer oligo encoding CR element was synthesized (IDTDNA) with seven SDPs, each with two possible nucleotides, in both desalted (gel filtration column) and HPLC-grade purification. The overall library therefore contained 128 possible permutations of the parent CR element structure. The library was Gibson assembled into a low copy pCKNCsfGFP vector (listed in Supplementary Table S4), upstream of *sfGFP* gene with constitutive expression (Ptac) creating the pCKCRlib vector library (primers listed in Supplementary Table S5). The library was transformed into the NEB T7 Express *E. coli* cell line with a library coverage x30. The transformations were pooled and cultured overnight until a mid-log growth phase was reached in culture tubes within 5 mL of LB media (supplemented with Kan50) incubated at 37 °C and shaking at 225 rpm; thereafter, an aliquot of the library was used to create glycerol stocks. After growing to the mid-log phase (OD_{600} 0.5 = ∼1 × 10^7 cells/mL), aliquots of the library were sorted on a FACS Aria fluorescence cell sorter. As an 'all-on' control, namely, NoCis (positive control), the CR element was modified to delete the 5′ portion of the helix removing any structural impediment to translation and inserted into the library. A negative control, namely, NEB5α cells (NEG), was included in the flow cytometry analysis.

For the first sort, an overall event rate of 8000 events/second was achieved using a primary detection threshold of (Flow Cytometry Standard) FCS-H = 2000 and gain/voltage settings = 10−12. The cell population was gated using a log plot for forward versus side light scatter (89−78%) of the total cell population (Supplementary Figure S1), and the fluorescence intensity of the gated cells is plotted in Figure 3B (with smoothing factor 50). The undiluted population was sorted two-ways (4000 events/second for each gate), and we collected 5 × 10^6 cells per each gate (amounted to a population 1 with 22−26% and a population 2 with 16−18% of the population) (Supplementary Figure S2). Subsequently, each of these two positive populations was sorted four-ways, with an overall event rate of 4000 events/second (i.e., 1000 events/seconds each gate) (Supplementary Figure S3). We collected 1 × 10^6 cells for each gate (amounted to each bin containing 22−26 and 17−18% of the two sorted populations, respectively), resulting in eight sorted final populations (namely, 1A, 1B, 1C, 1D, 2A, 2B, 2C, and 2D) diluted in 2 mL of PBS (Supplementary Figure S4). The instrument conducted one wash cycle between each sample, and the *sfGFP* expression was monitored using an excitation laser of 488 nm and an emission detection filter of 533/30 nm (FL-A channel). The data files were exported for analysis in FCS Express v.6.06.0040 (DeNovo Software). The fluorescence intensity of the sfGFP-expressing cells represents the maximal observable GFP fluorescence under these copy number, expression, and growth conditions. The DH5α served as background fluorescence in this channel. The samples were spun down, removing the PBS, resuspended in fresh media, and cultured overnight in 5 mL LB media supplemented with Kan50 at 37 °C in 15 mL Falcon tubes. Aliquots of the overnight culture were used for creating glycerol stocks and measuring fluorescence intensity on an Accuri BD autosampler, and the rest of the samples were miniprepped for plasmid extraction (Qiagen Spin Miniprep Kit). Plasmid concentration was determined using a dsDNA HS Qubit assay (Thermo-Fisher), and equal amounts of amplicon DNA were used before adding the barcodes and Illumina adapters (primers listed in Supplementary Table S3). PCR cleanup and concentration (ZymoResearch) were performed followed by gel purification (ZymoResearch); thereafter, the samples were pooled.[51,52]

The concentrations of the resulting multiplexed sample libraries were obtained using the Qubit dsDNA HS Assay (Thermo-Fisher Scientific, Cat. #Q32854). The average size and concentration of the library were determined using the Agilent High Sensitivity DNA Kit (Agilent, Cat. #5067-4626) and the Library Quantification Kit − Illumina/Universal Kit (KAPA Biosystems, KK4824), respectively. Each library was sequenced on approximately three percent of a different MiSeq Reagent Kit v3 (600-cycle) (Illumina, Cat. #MS-102-3003) to generate paired end 251 bp reads. Postsequencing, the barcoded Illumina sequence reads were demultiplexed by a custom script based on the barcode spacer and PCR primer (Supplementary Table S3). To identify and calculate the population variations in each sample pool, the demultiplexed reads were trimmed to match the amplicon size and normalized to the least number of reads recovered per sample. Each in silico normalized read pool was mapped to the riboregulator sequence (∼190 bp) with bwa v0.7.12[53] (parameters -B 1 -O 1 -L 100). The positions containing the randomized nucleotide sites were extracted, and the frequency of each combination was counted with a custom script and was visualized by R v3.1.2.[52] Illumina sequencing data were analyzed using in-house scripts to identify and calculate the

https://doi.org/10.1021/acssynbio.1c00638
ACS Synth. Biol. 2022, 11, 3216−3227

population variations in each pool. The 16 individual CR sequences, two from each pool, were selected based on their enrichment in that pool (Supplementary Table S6). These sequences were then synthesized as gBlocks (IDTDNA) for re-insertion into the low-copy pBLT-2_sfGFP and pBLT-2_CAT under constitutive expression (Ptac and T7A1, respectively) for validation using analytical flow cytometer fluorescence measurements.

The CR-1A1 sequence was obtained as a gBlock synthetic sequences (IDTDNA) and PCR amplified to include the overlapping ends with pBTL-2 vector[51] as well as the *sf GFP* and (primers listed in Supplementary Table S3). The pBTL-2 was digested with restriction enzymes BamHI (NEB) and EcoRV (NEB). The gBlock, sfGFP PCR product, and the digested vector were Gibson assembled using the NEBuilder HiFi Assembly kit (NEB) to create pBTL-2_Ptac_1A1_sfGFP plasmid (listed in Supplementary Table S4). To create other *cis*-repressed sfGFP plasmids, the pBTL-2_Ptac_1A1_sfGFP plasmid was digested with AatII (NEB) and BstBI (NEB) to remove the CR-1A1 sequence and was Gibson assembled with either the 1C2, 2B1, 2C1, 2D1, or NoCis CR gBlocks, resulting in pBTL1_ptac_(1C2, 2B1, 2C1, 2D1, or NoCis)_sfGFP plasmids, respectively. To create the *cis*-repressed CAT plasmids, the pBTL-2 was digested with restriction enzymes XbaI (NEB) and EcoRV (NEB). The T7A1 promoter sequence with *cat* gene was amplified from pETcoco2[31,55] using primers listed in Supplementary Table S3. The gBlock, T7A1_CAT PCR product, and the digested vector were Gibson assembled using the NEBuilder HiFi Assembly kit (NEB) to create pBTL-2_T7A1_CR_CAT plasmid (listed in Supplementary Table S4). All the plasmids were transformed into *P. putida* strains by electroporation[54] using a 1 mM cuvette at 1.6 kV, 25 μF, and 200 ohms (BioRad). Transformed cells were selected on LB agar plates containing Kan50, and a single colony was PCR confirmed, cultivated to make a glycerol stock, and stored at −80 °C.

Fluorescence Measurements Using a Plate Reader and a BD Accuri Flow Cytometer. Plasmids encoding CRs with the gene *sf GFP* were transformed into *P. putida* by electroporation. Two 5 mL cultures of 1× M9 media with Kan50 were inoculated using frozen glycerol stocks. After 16 h at 30 °C and 225 rpm, cells were analyzed for fluorescence intensity and absorbance. Whole cell absorbance (OD_{600}) and fluorescence (excitation = 480 nm, emission = 510 nm, cutoff = 495 nm) were acquired from 200 μL of samples in black, flat bottom optical grade 96-well plates (Corning) using a Molecular Devices SpectraMax M5 plate reader. Fluorescence intensity was normalized to absorbance (OD_{600}) in each well, and data reported represent three biological replicates.

For Accuri measurements, cells were grown in 5 mL LB medium for 16 h, then diluted 1:20 in 1× M9 media, and loaded into a black, flat bottom 96-well plate (Corning) for measuring fluorescence over a 24 h time-course. For the *P. putida* strains with genomic integrated CR with the *sf GFP* gene, the fluorescence intensity was measured using a BD Biosciences Accuri C6 benchtop flow cytometer fitted with a 96-well plate autosampler. 30,000 events per sample were collected on the slow fluidics setting using a primary detection threshold of FSC-H = 20,000. The FCS data files were exported for analysis in FCS Express v6.06.0040 (DeNovo Software). The fluorescence intensity of the sfGFP-expressing cultures represents the maximal observable sfGFP fluorescence under these copy number, activity, and growth conditions. The instrument conducted one wash cycle between each sample, and sfGFP activity was monitored using an excitation laser of 488 nm and an emission of detector filter 533/30 nm (FL1-A channel). The arithmetic mean fluorescence value of ∼500,000 cells based on forward and side scatter was used for the fluorescence plot. Strains with no CR but with *sf GFP* gene (NoCis) and *P. putida* KT2440 wild type (Con.) were used as positive and negative references for fluorescence measurements, respectively.

Plasmid Construction and Genomic Integration. A subset of the gBlock elements (10 in total) were assembled into the single-copy pETcoco2[55] vector to regulate the protein production level of the chloramphenicol acetyltransferase (*cat*) gene driven by the T7A1 promoter. The vectors were transformed into Neb5α to test for resistance to chloramphenicol (Cm, Fisher Scientific). Strains were grown overnight at 37 °C, and samples were diluted in fresh media to a final concentration 0.1 OD_{600}. The cells were grown in triplicate 5 mL of culture at increasing concentrations of Cm (0, 30, 60, 120, 240, 500, and 1000 μg/mL) in LB media for 6 h in the presence of 0.2% glucose to maintain the single-copy state of the vector.

The 5′ and 3′ homology arms flanking the intergenic region between the genes PP_2684[74] (1053 bp) and PP_2685[74] (993 bp) were PCR amplified from the KT2440 strain using KOD Hot Start polymerase (Millipore). These PCR fragments have a common 20 bp overlapping end to 3′ end of 5′ homology arm and 5′ end of *sf GFP* sequence (primers listed in Supplementary Table S5). Various CR elements were PCR amplified from the gBlocks. The *sf GFP* gene cassette was PCR amplified from plasmid pCKNCsfGFP. The homology arms, CRs, and *sf GFP* PCR products were Gibson assembled[38] into the suicide integration vector pk18mobsacB[19] using the NEBuilder HiFi Assembly kit (NEB). This created the pk18mobsacB_ptac_(1A1 or 1C2 or 2B1 or 2C1 or 2D1 or NoCis)_sfGFP plasmid for genomic integration (Supplementary Table S4). For *ppsA* integration vectors, 5′ and 3′ homology arms flanking the intergenic region between the genes PP_2081[74] and PP_2082[74] were PCR amplified from the KT2440 strain using KOD Hot Start polymerase (Millipore). The homology arms consisted of 773 bp of the PEP synthase regulatory protein, PP_2081 (223 bp of PP_2081's 5′ end was deleted to remove expression and therefore regulate the PpsA by the PsrP protein) and 1003 bp of PP_2082 (all primers listed in Supplementary Table S5). As described above, PCR amplified CRs with 20 bp overlap to the 3′ end of 5′ homology arm and 5′ end of *ppsA* were Gibson assembled into the suicide integration vector pk18mobsacB using the NEBuilder HiFi Assembly kit resulting in pk18mobsacb_Δpsrp_ptac_(1A1, 1C1, 1D1 or 2B2)_ppsA (Supplementary Table S4).

Gene integration in the *P. putida* KT2440-derived strain CJ442 (Supplementary Table S4) was accomplished by electroporation of the pk18mobsacB_ptac_ (1A1 or 1C1 or 1D1 or 2B2) _ppsA plasmids (Supplementary Table S4). Briefly, chromosomal integration by homologous recombination was selected on LB agar plates supplemented with Kan50. Colonies were counter-selected for a second cross-over event to remove the plasmid from the genome on yeast extract and tryptone agar plates supplemented with 25% sucrose (Merck), as described previously.[38,39] Insertion was confirmed by PCR amplification using primers F_Dikinase_cis_screen and F_Dikinase_cis_screen (listed in Supplementary Table S5) that bind outside of the regions used for CR integration. More

https://doi.org/10.1021/acssynbio.1c00638
ACS Synth. Biol. 2022, 11, 3216−3227

detailed descriptions can be found in the Supplementary Material.

Muconate Production from Glucose in a Shake Flask. *P. putida* strains were evaluated for muconate production using shake flasks. 3−5 mL of LB overnight cultures were grown in 15 mL Falcon tubes (Fischer) in an incubating shaker at 225 rpm, 30 °C for 16 h. Cultures were centrifuged and resuspended in fresh 1 mL of LB and used for inoculating 5 mL of LB in 15 mL Falcon tube to the OD_{600} of 0.2 and cultivated at 225 rpm, 30 °C for 4 h. Cultures were centrifuged and resuspended in 1 mL 1× M9 medium supplemented with 30 mM glucose. This was used for inoculating 25 mL 1× M9 medium (supplemented with 30 mM glucose) to the final OD_{600} of 0.05 in 125 mL baffled shake flasks and cultivated in an incubating shaker at 225 rpm, 30 °C. Flasks were continually monitored by measuring OD_{600}.

Quantification of Glucose and Muconate Concentrations Using High-Performance Liquid Chromatography (HPLC). To measure muconate concentration, the culture samples were collected at various time points and centrifuged at 16,000 rpm for one min. The supernatants were transferred to a 0.22 μm filtration spin column (Corning Costar Spin-X with cellulose acetate membrane) and centrifuged, and the filtrate was transferred to a 96-well PCR plate (Thermo-Scientific) covered with a clear microseal (Biorad) for analysis using an Agilent 1100 series HPLC system. The samples were injected on a SUPELCOGEL H Column (SUPELCO) using HPLC-grade 0.1% (v/v) H_2SO_4 (Fisher Scientific) at a flow rate of 0.5 mL/min as a mobile phase for 40 min[39]. A refractive index detector (RID) set at 258 nm wavelength was used to quantify muconate, 2-ketogluconate and glucose concentrations. The temperatures of both the column and RID were maintained at 45 °C. Peak areas for glucose and muconate were integrated using Agilent Chemstation software and compared to standard curves made using HPLC-grade glucose (Sigma) and *cis*, *cis*-muconate samples (Sigma).

■ ASSOCIATED CONTENT

Supporting Information

The Supporting Information is available free of charge at https://pubs.acs.org/doi/10.1021/acssynbio.1c00638.

> Histogram plots based on analyses performed by flow cytometry for the positive control ('NoCis') negative control ('DH5a', DH5α cells without vector), sorted CR library and eight isolated subpopulations (1A, 1B, 1C, 1D, 2A, 2B, 2C, and 2D) (Figures S1−S5), strains, plasmids, and oligonucleotides used in this study (Tables S1−S6) (PDF)

■ AUTHOR INFORMATION

Corresponding Author

Taraka Dale − *Bioscience Division, Los Alamos National Laboratory, Los Alamos, New Mexico 87545, United States*; Email: tdale@lanl.gov

Authors

Naresh Pandey − *Bioscience Division, Los Alamos National Laboratory, Los Alamos, New Mexico 87545, United States;* Present Address: Andes Ag, 1555 Park Avenue, Emeryville, California 94608, United States

Steffi A. Davison − *Bioscience Division, Los Alamos National Laboratory, Los Alamos, New Mexico 87545, United States*

Malathy Krishnamurthy − *Bioscience Division, Los Alamos National Laboratory, Los Alamos, New Mexico 87545, United States;* Present Address: Henry M. Jackson Foundation for the Advancement of Military Medicine, 6720A Rockledge Drive, Bethesda, Maryland 20817, United States

Daniel S. Trettel − *Bioscience Division, Los Alamos National Laboratory, Los Alamos, New Mexico 87545, United States*

Chien-Chi Lo − *Bioscience Division, Los Alamos National Laboratory, Los Alamos, New Mexico 87545, United States*

Shawn Starkenburg − *Bioscience Division, Los Alamos National Laboratory, Los Alamos, New Mexico 87545, United States*

Katherine L. Wozniak − *Chemistry Division, Los Alamos National Laboratory, Los Alamos, New Mexico 87545, United States*

Theresa L. Kern − *Bioscience Division, Los Alamos National Laboratory, Los Alamos, New Mexico 87545, United States*

Sean D. Reardon − *Bioscience Division, Los Alamos National Laboratory, Los Alamos, New Mexico 87545, United States;* Present Address: Department of Chemistry and Biochemistry, University of California San Diego, La Jolla, California 92093, United States

Clifford J. Unkefer − *Bioscience Division, Los Alamos National Laboratory, Los Alamos, New Mexico 87545, United States*

Scott P. Hennelly − *Bioscience Division, Los Alamos National Laboratory, Los Alamos, New Mexico 87545, United States;* Present Address: Ntx Bio, 7701 Innovation Way, Rio Rancho, New Mexico 87144, United States

Complete contact information is available at: https://pubs.acs.org/10.1021/acssynbio.1c00638

Funding

This work was supported by the U.S. Department of Energy through the Los Alamos National Laboratory. Los Alamos National Laboratory is operated by Triad National Security, LLC, for the National Nuclear Security Administration of U.S. Department of Energy (Contract No. 89233218CNA000001). This material is based upon work supported by the U.S. Department of Energy, Office of Energy Efficiency and Renewable Energy (EERE), specifically the Bioenergy Technologies Office, Agile BioFoundry under contract number NL0032182. Research presented in this article was also supported by the Laboratory Directed Research and Development program of Los Alamos National Laboratory under project number 20130091DR. This article is approved for Los Alamos Unlimited Release under LA-UR-21-32232.

Notes

The authors declare no competing financial interest.

■ ACKNOWLEDGMENTS

This work was supported by the U.S. Department of Energy through the Los Alamos National Laboratory. Los Alamos National Laboratory is operated by Triad National Security, LLC, for the National Nuclear Security Administration of U.S. Department of Energy (Contract No. 89233218CNA000001). This material is based upon work supported by the U.S. Department of Energy, Office of Energy Efficiency and Renewable Energy (EERE), specifically the Bioenergy

Technologies Office, Agile BioFoundry under contract number NL0032182. Research presented in this article was also supported by the Laboratory Directed Research and Development program of Los Alamos National Laboratory under project number 20130091DR. This article is approved for Los Alamos Unlimited Release under LA-UR-21-32232. Special thanks to Cheryl Gleasner for technical assistance with Illumina sequencing, Claire Sanders for technical assistance with flow cytometry measurements, and Ramesh Jha for reading and thoughtful comments.

■ ABBREVIATIONS

Ac-CoA, acetyl-Coenzyme A; AsbF, a 3-DHS dehydrase; AroY/EcdB, a protocatechuate decarboxylase; asRNA, 'antisense' sRNA; CR, *cis*-repressor; MA, *cis*,*cis*-muconate; DAHP, 3-deoxy-D-arabinoheptulosonate 7-phosphate; E4P, erythrose-4-P; *E. coli*, *Escherichia coli*; FACS, fluorescence-activated cell sorting; FI, fluorescence intensity; FCS, Flow Cytometry Standard; F6P, fructose-6-P; HPLC, high-performance liquid chromatography; G6P, glucose-6-P; Kan50, 50 μg/mL kanamycin; KDPG, 2-keto-3-deoxy-6-phosphogluconate; 2-KG, 2-ketogluconate; LB, Luria broth; PpsA, phosphoenolpyruvate synthase enzyme; *P. putida*, *Pseudomonas putida*; PEP, phosphoenolpyruvate; PYR, pyruvate; sfGFP, superfolded green fluorescent protein; SDP, semidegenerate position; RBS, ribosomal binding site; sRNA, noncoding RNAs; RID, refractive index detector; 6PG, 6-phosphogluconate

■ REFERENCES

(1) Lu, T. K.; Khalil, A. S.; Collins, J. J. Next-Generation Synthetic Gene Networks. *Nat. Biotechnol.* **2009**, *27*, 1139−1150.
(2) Cameron, D. E.; Bashor, C. J.; Collins, J. J. A Brief History of Synthetic Biology. *Nat. Rev. Microbiol.* **2014**, *12*, 381−390.
(3) Kent, R.; Dixon, N. Contemporary Tools for Regulating Gene Expression in Bacteria. *Trends Biotechnol.* **2020**, *38*, 316−333.
(4) Du, J.; Shao, Z.; Zhao, H. Engineering Microbial Factories for Synthesis of Value-Added Products. *J. Ind. Microbiol. Biotechnol.* **2011**, *38*, 873−890.
(5) Beckham, G. T.; Johnson, C. W.; Karp, E. M.; Salvachúa, D.; Vardon, D. R. Opportunities and Challenges in Biological Lignin Valorization. *Curr. Opin. Biotechnol.* **2016**, *42*, 40−53.
(6) Linger, J. G.; Vardon, D. R.; Guarnieri, M. T.; Karp, E. M.; Hunsinger, G. B.; Franden, M. A.; Johnson, C. W.; Chupka, G.; Strathmann, T. J.; Pienkos, P. T.; Beckham, G. T. Lignin Valorization through Integrated Biological Funneling and Chemical Catalysis. *Proc. Natl. Acad. Sci. U. S. A.* **2014**, *111*, 12013−12018.
(7) Ueno, K.; Sakai, Y.; Shono, C.; Sakamoto, I.; Tsukakoshi, K.; Hihara, Y.; Sode, K.; Ikebukuro, K. Applying a Riboregulator as a New Chromosomal Gene Regulation Tool for Higher Glycogen Production in *Synechocystis* Sp. PCC 6803. *Appl. Microbiol. Biotechnol.* **2017**, *101*, 8465−8474.
(8) Kim, O. D.; Rocha, M.; Maia, P. A Review of Dynamic Modeling Approaches and Their Application in Computational Strain Optimization for Metabolic Engineering. *Front. Microbiol.* **2018**, *9*, 1−22.
(9) Wu, G.; Yan, Q.; Jones, J. A.; Tang, Y. J.; Fong, S. S.; Koffas, M. A. G. Metabolic Burden: Cornerstones in Synthetic Biology and Metabolic Engineering Applications. *Trends Biotechnol.* **2016**, *34*, 652−664.
(10) Han, Y.; Zhang, F. Control Strategies to Manage Trade-Offs during Microbial Production. *Curr. Opin. Biotechnol.* **2020**, *66*, 158−164.
(11) Chaves, J. E.; Wilton, R.; Gao, Y.; Munoz, N. M.; Burnet, M. C.; Schmitz, Z.; Rowan, J.; Burdick, L. H.; Elmore, J.; Guss, A.; Close, D.; Magnuson, J. K.; Burnum-Johnson, K. E.; Michener, J. K. Evaluation of Chromosomal Insertion Loci in the *Pseudomonas putida* KT2440 Genome for Predictable Biosystems Design. *Metab. Eng. Commun.* **2020**, *11*, No. e00139.
(12) Johnson, C. W.; Salvachúa, D.; Rorrer, N. A.; Black, B. A.; Vardon, D. R.; St. John, P. C.; Cleveland, N. S.; Dominick, G.; Elmore, J. R.; Grundl, N.; Khanna, P.; Martinez, C. R.; Michener, W. E.; Peterson, D. J.; Ramirez, K. J.; Singh, P.; VanderWall, T. A.; Wilson, A. N.; Yi, X.; Biddy, M. J.; Bomble, Y. J.; Guss, A. M.; Beckham, G. T. Innovative Chemicals and Materials from Bacterial Aromatic Catabolic Pathways. *Joule* **2019**, *3*, 1523−1537.
(13) Johnson, C. W.; Salvachúa, D.; Khanna, P.; Smith, H.; Peterson, D. J.; Beckham, G. T. Enhancing Muconic Acid Production from Glucose and Lignin-Derived Aromatic Compounds via Increased Protocatechuate Decarboxylase Activity. *Metab. Eng. Commun.* **2016**, *3*, 111−119.
(14) Liu, S.; Wang, P. The Sequence of the Ribosomal Binding Site Controls the Gene Expression in Brucella. *Research Square* **2021**, 1−22.
(15) Aparicio, T.; Nyerges, A.; Martínez-García, E.; de Lorenzo, V. High-Efficiency Multi-Site Genomic Editing of *Pseudomonas putida* through Thermoinducible SsDNA Recombineering. *iScience*, 2020, 23, 100946. DOI: 10.1016/j.isci.2020.100946.
(16) Hallberg, Z. F.; Su, Y.; Kitto, R. Z.; Hammond, M. C. Engineering and *in Vivo* Applications of Riboswitches. *Annu. Rev. Biochem.* **2017**, *86*, 515−539.
(17) Groher, F.; Suess, B. Synthetic Riboswitches - A Tool Comes of Age. *Biochim. Biophys. Acta, Gene Regul. Mech.* **2014**, *1839*, 964−973.
(18) Yoo, S. M.; Jung, S. W.; Yeom, J.; Lee, S. Y.; Na, D. Tunable Gene Expression System Independent of Downstream Coding Sequence. *ACS Synth. Biol.* **2020**, *9*, 2998−3007.
(19) Jung, S.-W.; Yeom, J.; Park, J. S.; Yoo, S. M. Recent Advances in Tuning the Expression and Regulation of Genes for Constructing Microbial Cell Factories. *Biotechnol. Adv.* **2021**, *50*, No. 107767.
(20) Saito, K.; Green, R.; Buskirk, A. R. Translational Initiation in *E. coli* Occurs at the Correct Sites Genome-Wide in the Absence of Mrna-Rrna Base-Pairing. *eLife* **2020**, *9*, 1−19.
(21) Komarova, E. S.; Chervontseva, Z. S.; Osterman, I. A.; Evfratov, S. A.; Rubtsova, M. P.; Zatsepin, T. S.; Semashko, T. A.; Kostryukova, E. S.; Bogdanov, A. A.; Gelfand, M. S.; Dontsova, O. A.; Sergiev, P. V. Influence of the Spacer Region between the Shine−Dalgarno Box and the Start Codon for Fine-Tuning of the Translation Efficiency in *Escherichia coli*. *Microb. Biotechnol.* **2020**, *13*, 1254−1261.
(22) Eriksen, M.; Sneppen, K.; Pedersen, S.; Mitarai, N. Occlusion of the Ribosome Binding Site Connects the Translational Initiation Frequency, mRNA Stability and Premature Transcription Termination. *Front. Microbiol.* **2017**, *8*, 1−7.
(23) Horga, L. G.; Halliwell, S.; Castiñeiras, T. S.; Wyre, C.; Matos, C. F. R. O.; Yovcheva, D. S.; Kent, R.; Morra, R.; Williams, S. G.; Smith, D. C.; Dixon, N. Tuning Recombinant Protein Expression to Match Secretion Capacity. *Microb. Cell Fact.* **2018**, *17*, 1−18.
(24) Ding, N.; Yuan, Z.; Zhang, X.; Chen, J.; Zhou, S.; Deng, Y. Programmable Cross-Ribosome-Binding Sites to Fine-Tune the Dynamic Range of Transcription Factor-Based Biosensor. *Nucleic Acids Res.* **2020**, *48*, 10602−10613.
(25) Elmore, J. R.; Furches, A.; Wolff, G. N.; Gorday, K.; Guss, A. M. Development of a High Efficiency Integration System and Promoter Library for Rapid Modification of *Pseudomonas putida* KT2440. *Metab. Eng. Commun.* **2017**, *5*, 1−8.
(26) Spöring, M.; Finke, M.; Hartig, J. S. Aptamers in RNA-Based Switches of Gene Expression. *Curr. Opin. Biotechnol.* **2020**, *63*, 34−40.
(27) Lim, H. N.; Lee, Y.; Hussein, R. Fundamental Relationship between Operon Organization and Gene Expression. *Proc. Natl. Acad. Sci. U. S. A.* **2011**, *108*, 10626−10631.
(28) Quax, T. E. F.; Wolf, Y. I.; Koehorst, J. J.; Wurtzel, O.; vanderOost, R.; Ran, W.; Blombach, F.; Makarova, K. S.; Brouns, S. J. J.; Forster, A. C.; Wagner, E. G. H.; Sorek, R.; Koonin, E. V.; vanderOost, J. Differential Translation Tunes Uneven Production of Operon-Encoded Proteins. *Cell Rep.* **2013**, *4*, 938−944.
(29) Valeri, J. A.; Collins, K. M.; Ramesh, P.; Alcantar, M. A.; Lepe, B. A.; Lu, T. K.; Camacho, D. M. Sequence-to-Function Deep

Learning Frameworks for Engineered Riboregulators. *Nat. Commun.* **2020**, *11*, 1−14.
(30) Thiel, K.; Mulaku, E.; Dandapani, H.; Nagy, C.; Aro, E. M.; Kallio, P. Translation Efficiency of Heterologous Proteins Is Significantly Affected by the Genetic Context of RBS Sequences in Engineered *Cyanobacterium synechocystis* Sp. PCC 6803. *Microb. Cell Fact.* **2018**, *17*, 1−12.
(31) Krishnamurthy, M.; Hennelly, S. P.; Dale, T.; Starkenburg, S. R.; Martí-Arbona, R.; Fox, D. T.; Twary, S. N.; Sanbonmatsu, K. Y.; Unkefer, C. J. Tunable Riboregulator Switches for Post-Transcriptional Control of Gene Expression. *ACS Synth. Biol.* **2015**, *4*, 1326−1334.
(32) Davidson, E. A.; Ellington, A. D. Engineering Regulatory RNAs. *Trends Biotechnol.* **2005**, *23*, 109−112.
(33) Pédelacq, J. D.; Cabantous, S.; Tran, T.; Terwilliger, T. C.; Waldo, G. S. Engineering and Characterization of a Superfolder Green Fluorescent Protein. *Nat. Biotechnol.* **2006**, *24*, 79−88.
(34) Lee, Y.; Park, E. J.; Yu, S. S.; Kim, D. K.; Kim, S. Improved Expression of Vascular Endothelial Growth Factor by Naked DNA in Mouse Skeletal Muscles: Implication for Gene Therapy of Ischemic Diseases. *Biochem. Biophys. Res. Commun.* **2000**, *272*, 230−235.
(35) Bentley, G. J.; Narayanan, N.; Jha, R. K.; Salvachúa, D.; Elmore, J. R.; Peabody, G. L.; Black, B. A.; Ramirez, K.; De Capite, A.; Michener, W. E.; Werner, A. Z.; Klingeman, D. M.; Schindel, H. S.; Nelson, R.; Foust, L.; Guss, A. M.; Dale, T.; Johnson, C. W.; Beckham, G. T. Engineering Glucose Metabolism for Enhanced Muconic Acid Production in *Pseudomonas putida* KT2440. *Metab. Eng.* **2020**, *59*, 64−75.
(36) Jha, R. K.; Kern, T. L.; Kim, Y.; Tesar, C.; Jedrzejczak, R.; Joachimiak, A.; Strauss, C. E. M. A Microbial Sensor for Organophosphate Hydrolysis Exploiting an Engineered Specificity Switch in a Transcription Factor. *Nucleic Acids Res.* **2016**, *44*, 8490−8500.
(37) Jha, R. K.; Bingen, J. M.; Johnson, C. W.; Kern, T. L.; Khanna, P.; Trettel, D. S.; Strauss, C. E. M.; Beckham, G. T.; Dale, T. A Protocatechuate Biosensor for *Pseudomonas putida* KT2440 via Promoter and Protein Evolution. *Metab. Eng. Commun.* **2018**, *6*, 33−38.
(38) Jha, R. K.; Narayanan, N.; Pandey, N.; Bingen, J. M.; Kern, T. L.; Johnson, C. W.; Strauss, C. E. M.; Beckham, G. T.; Hennelly, S. P.; Dale, T. Sensor-Enabled Alleviation of Product Inhibition in Chorismate Pyruvate-Lyase. *ACS Synth. Biol.* **2019**, *8*, 775−786.
(39) Johnson, C. W.; Beckham, G. T. Aromatic Catabolic Pathway Selection for Optimal Production of Pyruvate and Lactate from Lignin. *Metab. Eng.* **2015**, *28*, 240−247.
(40) Li, W.; Shen, X.; Wang, J.; Sun, X.; Yuan, Q. Engineering Microorganisms for the Biosynthesis of Dicarboxylic Acids. *Biotechnol. Adv.* **2021**, *48*, No. 107710.
(41) Nelson, K. E.; Weinel, C.; Paulsen, I. T.; Dodson, R. J.; Hilbert, H.; Martins Dos Santos, V. A. P.; Fouts, D. E.; Gill, S. R.; Pop, M.; Holmes, M.; Brinkac, L.; Beanan, M.; DeBoy, R. T.; Daugherty, S.; Kolonay, J.; Madupu, R.; Nelson, W.; White, O.; Peterson, J.; Khouri, H.; Hance, I.; Lee, P. C.; Holtzapple, E.; Scanlan, D.; Tran, K.; Moazzez, A.; Utterback, T.; Rizzo, M.; Lee, K.; Kosack, D.; Moestl, D.; Wedler, H.; Lauber, J.; Stjepandic, D.; Hoheisel, J.; Straetz, M.; Heim, S.; Kiewitz, C.; Eisen, J. A.; Timmis, K. N.; Düsterhöft, A.; Tümmler, B.; Fraser, C. M. Erratum: Complete Genome Sequence and Comparative Analysis of the Metabolically Versatile *Pseudomonas putida* KT2440. *Environ. Microbiol.* **2003**, *5*, 630.
(42) Yi, J.; Li, K.; Draths, K. M.; Frost, J. W. Modulation of Phosphoenolpyruvate Synthase Expression Increases Shikimate Pathway Product Yields in *E. coli*. *Biotechnol. Prog.* **2002**, *18*, 1141−1148.
(43) Hogema, B. M.; Arents, J. C.; Bader, R.; Eijkemans, K.; Yoshida, H.; Takahashi, H.; Aiba, H.; Postma, P. W. Inducer Exclusion in *Escherichia coli* by Non-PTS Substrates: The Role of the PEP to Pyruvate Ratio in Determining the Phosphorylation State of Enzyme IIA(Glc). *Mol. Microbiol.* **1998**, *30*, 487−498.
(44) Liu, K.; Hu, H.; Wang, W.; Zhang, X. Genetic Engineering of *Pseudomonas chlororaphis* GP72 for the Enhanced Production of 2-Hydroxyphenazine. *Microb. Cell Fact.* **2016**, *15*, 1−12.
(45) Chen, J.; Mitra, R.; Zhang, S.; Zuo, Z.; Lin, L.; Zhao, D.; Xiang, H.; Han, J. Unusual Phosphoenolpyruvate (PEP) Synthetase-Like Protein Crucial to Enhancement of Polyhydroxyalkanoate Accumulation in *Haloferax mediterranei* Revealed by Dissection of PEP-Pyruvate Interconversion Mechanism. *Appl. Environ. Microbiol.* **2019**, *85*, e00984−e00919.
(46) Nechooshtan, G.; Elgrably-weiss, M.; Sheaffer, A.; Westhof, E.; Altuvia, S. A pH-Responsive Riboregulator. 2009, 2650−2662, DOI: 10.1101/gad.552209.terminator.
(47) Goodwine, J.; Gil, J.; Doiron, A.; Valdes, J.; Solis, M.; Higa, A.; Davis, S.; Sauer, K. Pyruvate-Depleting Conditions Induce Biofilm Dispersion and Enhance the Efficacy of Antibiotics in Killing Biofilms *in Vitro* and *in Vivo*. *Sci. Rep.* **2019**, *9*, 1−16.
(48) Moxley, W. C.; Eiteman, M. A. Pyruvate Production by *Escherichia coli* Using Pyruvate Dehydrogenase Variants. *Appl. Environ. Microbiol.* **2021**, *87*, No. e0048721.
(49) Hawkins, J. S.; Silvis, M. R.; Koo, B. M.; Peters, J. M.; Osadnik, H.; Jost, M.; Hearne, C. C.; Weissman, J. S.; Todor, H.; Gross, C. A. Mismatch-CRISPRi Reveals the Co-Varying Expression-Fitness Relationships of Essential Genes in *Escherichia coli* and *Bacillus subtilis*. *Cell Syst.* **2020**, 523−535.e9.
(50) Salis, H. M.; Mirsky, E. A.; Voigt, C. A. Automated Design of Synthetic Ribosome Binding Sites to Control Protein Expression. *Nat. Biotechnol.* **2009**, *27*, 946−950.
(51) Chen, M.-J.; Kreuter, J. Y.-T. K. Nanoparticles and Microparticles for Drug and Vaccine Delivery. *J. Anat.* **1996**, *189*, 503−505.
(52) Bunn, A. *An Introduction to DplR*, 2019; p 3.
(53) Li, H. *Aligning Sequence Reads , Clone Sequences and Assembly Contigs with BWA-MEM*, 2013; pp 1−3.
(54) Choi, K. R.; Cho, J. S.; Cho, I. J.; Park, D.; Lee, S. Y. Markerless Gene Knockout and Integration to Express Heterologous Biosynthetic Gene Clusters in *Pseudomonas putida*. *Metab. Eng.* **2018**, *47*, 463−474.
(55) Sektas, M.; Szybalski, W. Novel Single-Copy PETcoco™ Vector with Dual Controls for Amplification and Expression. *Innovations* **2002**, *6*−*8*, 6−8.

https://doi.org/10.1021/acssynbio.1c00638
ACS Synth. Biol. 2022, 11, 3216−3227